AGU PUBLICATIONS

JGR

Journal of Geophysical Research: Atmospheres

RESEARCH ARTICLE
10.1002/2016JD025437

Key Points:
- Continuous carbonyl sulfide measurements are presented for the North Atlantic marine boundary layer during fall and winter of 2014 and 2015
- Variations in carbonyl sulfide concentrations are shown to be directly proportionate to an air mass' solar radiation history
- Changes in the latitude of jet stream can affect the aqueous to atmosphere concentration gradient and the direction of the marine flux

Supporting Information:
- Supporting Information S1
- Table S1
- Table S2

Correspondence to:
M. Berkelhammer,
berkelha@uic.edu

Citation:
Berkelhammer, M., H. C. Steen-Larsen, A. Cosgrove, A. J. Peters, R. Johnson, M. Hayden, and S. A. Montzka (2016), Radiation and atmospheric circulation controls on carbonyl sulfide concentrations in the marine boundary layer, *J. Geophys. Res. Atmos.*, *121*, 13,113–13,128, doi:10.1002/2016JD025437.

Received 31 MAY 2016
Accepted 17 OCT 2016
Accepted article online 24 OCT 2016
Published online 8 NOV 2016

Radiation and atmospheric circulation controls on carbonyl sulfide concentrations in the marine boundary layer

M. Berkelhammer[1], H. C. Steen-Larsen[2], A. Cosgrove[1], A. J. Peters[3], R. Johnson[3], M. Hayden[3], and S. A. Montzka[4]

[1]Department of Earth and Environmental Sciences, University of Illinois at Chicago, Chicago, Illinois, USA, [2]Centre for Ice and Climate, University of Copenhagen, Copenhagen, Denmark, [3]Bermuda Institute of Ocean Sciences, St. Georges, Bermuda, [4]National Oceanic and Atmospheric Administration, Boulder, Colorado, USA

Abstract A potential closure of the global carbonyl sulfide (COS or OCS) budget has recently been attained through a combination of remote sensing, modeling, and extended surface measurements. However, significant uncertainties in the spatial and temporal dynamics of the marine flux still persist. In order to isolate the terrestrial photosynthetic component of the global atmospheric OCS budget, tighter constraints on the marine flux are needed. We present 6 months of nearly continuous in situ OCS concentrations from the North Atlantic during the fall and winter of 2014–2015 using a combination of research vessel and fixed tower measurements. The data are characterized by synoptic-scale ~100 pmol mol^{-1} variations in marine boundary layer air during transitions from subtropical to midlatitude source regions. The synoptic OCS variability is shown here to be a linear function of the radiation history along an air parcel's trajectory with no apparent sensitivity to the chlorophyll concentration of the surface waters that the air mass interacted with. This latter observation contradicts expectations and suggests a simple radiation limitation for the combined direct and indirect marine OCS emissions. Because the concentration of OCS in the marine boundary layer is so strongly influenced by an air parcel's history, marine and atmospheric concentrations would rarely be near equilibrium and thus even if marine production rates are held constant at a given location, the ocean-atmosphere flux would be sensitive to changes in atmospheric circulation alone. We hypothesize that changes in atmospheric circulation including latitudinal shifts in the storm tracks could affect the marine flux through this effect.

1. Introduction

The largest global source of atmospheric carbonyl sulfide (OCS or COS) is direct and indirect marine emissions [e.g., *Xu et al.*, 2001; *Kettle et al.*, 2002; *Von Hobe et al.*, 2001; *Berry et al.*, 2013; *Weiss et al.*, 1995; *Uher and Andreae*, 1996, 1997; *Launois et al.*, 2015]. This is because, on the global scale, photoproduction and dark production rates in the surface ocean and atmospheric oxidation of dimethyl sulfide (DMS) and carbon disulfide (CS_2) to OCS in the atmosphere exceed the rate of hydrolysis into the surface ocean [*Zepp and Andreae*, 1994; *Von Hobe et al.*, 1999; *Mihalopoulos et al.*, 1992; *Cutter et al.*, 2004; *Andreae and Ferek*, 1992; *Kettle et al.*, 2002]. However, it is not uncommon during periods when production rates are low or under conditions of low radiation for hydrolysis to exceed emissions and the ocean to act as a temporary or regional sink [*Ulshöfer et al.*, 1995; *Johnson and Harrison*, 1986; *Xu et al.*, 2001; *Weiss et al.*, 1995]. The lack of a secular trend in atmospheric OCS concentrations since 2000 suggests that the ocean flux is globally stable [*Berry et al.*, 2013; *Montzka et al.*, 2007] or that the major source (i.e., marine) and sink (i.e., vegetation) terms are coupled in such a way as to remain balanced with respect to one another. However, rising regional or global SSTs, retreat or expansion of sea ice, and/or changes in ocean productivity could shift the magnitude of the global marine flux and the sign of regional fluxes and lead to a change in atmospheric concentrations [*Weiss et al.*, 1995].

The processes that control the magnitude of the marine flux have been studied for decades [e.g., *Ferek and Andreae*, 1983; *Johnson and Harrison*, 1986; *Andreae and Ferek*, 1992]. Initially, this inquiry was motivated by the global climate impacts that a change in the marine flux would induce through its effect on stratospheric aerosols and global albedo [*Crutzen*, 1976]. To this end, numerous efforts to develop global estimates of the marine flux from ship campaigns and incubation experiments were conducted. These sparse data, however, are ultimately insufficient to support the interpretation of intensive [*Campbell et al.*, 2008] and long-term

efforts to monitor OCS at terrestrial sites [*Montzka et al.*, 2007] where real-time and regional marine flux data would greatly increase the robustness of atmospheric transport simulations [*Berry et al.*, 2013]. Further, an understanding of the dynamics of the ocean flux and its coupling with the atmosphere is needed to interpret the meaning of past secular variability in atmospheric OCS concentrations derived from ice core records [*Aydin et al.*, 2014, 2016]. Trends in past OCS concentrations (prior to anthropogenic emissions [*Montzka et al.*, 2004]) may reflect changes in either terrestrial vegetation or marine production (or both), but it is currently difficult to partition these drivers without better constraints on the factors that influence these fluxes.

The direct ocean to atmosphere flux, again the largest global source, is modeled according to the following general equation:

$$F_{OCS} = K \cdot \left(OCS_{aq} - \frac{OCS_{atmosphere}}{H} \right) \quad (1)$$

where F is the flux in pmol m^{-2} s^{-1}, K is the piston velocity in m s^{-1}, H is the Henry's law constant, and subscripts *aq* and *atmosphere* refer to the concentration (in pmol m^{-3}) of dissolved and atmospheric OCS concentrations, respectively [*Andreae and Ferek*, 1992]. Both the Henry's law constant (a function of temperature) [*Johnson and Harrison*, 1986] and piston velocity (a function of wind speed and temperature) are relatively well established [*Launois et al.*, 2015]. The OCS_{aq} term is modeled as the difference between the sum of photoproduction and dark production, hydrolysis, and mixing. The hydrolysis rate, as with Henry's law constant, has been experimentally derived and well constrained [*Elliott et al.*, 1989]. Photoproduction is modeled either simply as a function of incident UV radiation multiplied by a quantum yield term [*Uher and Andreae*, 1997] or with an explicit consideration of the concentration of chromophoric dissolved organic matter (CDOM), which is used as a generic proxy for organic OCS precursors [*Weiss et al.*, 1995; *Uher and Andreae*, 1996, 1997; *Zepp and Andreae*, 1994]. Dark production, which can account for more than half of total production [*Cutter et al.*, 2004], is a function of temperature and CDOM through a relationship established by *Von Hobe et al.* [2001]. Global or regional estimates of photoproduction and dark production further rely on a relationship between CDOM and ocean color, which enables global production rates to be estimated through remote sensing [*Preiswerk and Najjar*, 2000]. The expected concentrations of dissolved OCS that are predicted from this hierarchy of empirical models agree to a first order with isolated shipboard measurements that now span the Atlantic [*Xu et al.*, 2001; *Ulshöfer et al.*, 1995; *Von Hobe et al.*, 1999, 2001; *Andreae and Ferek*, 1992; *Cutter et al.*, 2004], Indian [*Mihalopoulos et al.*, 1992] and Pacific Oceans [*Johnson and Harrison*, 1986; *Ferek and Andreae*, 1983; *Weiss et al.*, 1995]. *Kettle et al.* [2002] used a form of these equations to generate the first global simulations of the atmospheric OCS cycle, which suggested a total annual marine flux of 279 Gg S yr^{-1}. When revised estimates of the magnitude of the global vegetation sink became available [*Suntharalingam et al.*, 2008; *Sandoval-Soto et al.*, 2005], it was suggested by *Berry et al.* [2013] that existing estimates of the marine flux were underestimated by a factor of 2 or more. The authors of this latter study suggested the presence of a large missing tropical marine source, which was potentially corroborated using global remote sensing of tropospheric OCS concentrations [*Kuai et al.*, 2015]. However, confirming the presence of such a large flux from the tropical ocean requires direct measurements.

Part of the challenge in estimating marine fluxes from scarce measurements is that the organic pathways for OCS precursors are complex and difficult to generalize across ocean basins [*Flöck et al.*, 1997]. This is because OCS is not only produced directly but also through multiple indirect pathways, chiefly the atmospheric oxidation of DMS and CS_2 [*Chin and Davis*, 1993; *Xie and Moore*, 1999], which may account for more OCS than the total direct emission flux. While the marine flux of both of these gases, like OCS, is influenced by radiation and CDOM, the production rates and factors that limit their emissions are distinct from one another. For example, DMS is both produced and consumed through biologic pathways, which can lead to nonlinear responses to climate factors influencing productivity [*Levine et al.*, 2015]. Across broad scales, some of the complexity can be ignored and these indirect OCS sources follow predictable relationships with SST and radiation [*Vallina and Simó*, 2007; *Chin and Davis*, 1993]. However, even if the emissions of these gases can be accurately predicted, a conversion rate to OCS may not be constant, though this is typically an assumption made when modeling the marine flux (e.g., 0.81 for CS_2 and 0.007 for DMS [*Chin and Davis*, 1993; *Barnes et al.*, 1994]).

We focus hereafter on the processes that control atmospheric concentration of OCS in the marine boundary layer as an aggregate of the direct and indirect sources of marine OCS. On average, the concentration in the marine boundary layer is ~500 pmol mol^{-1} [*Launois et al.*, 2015], though this value can range from

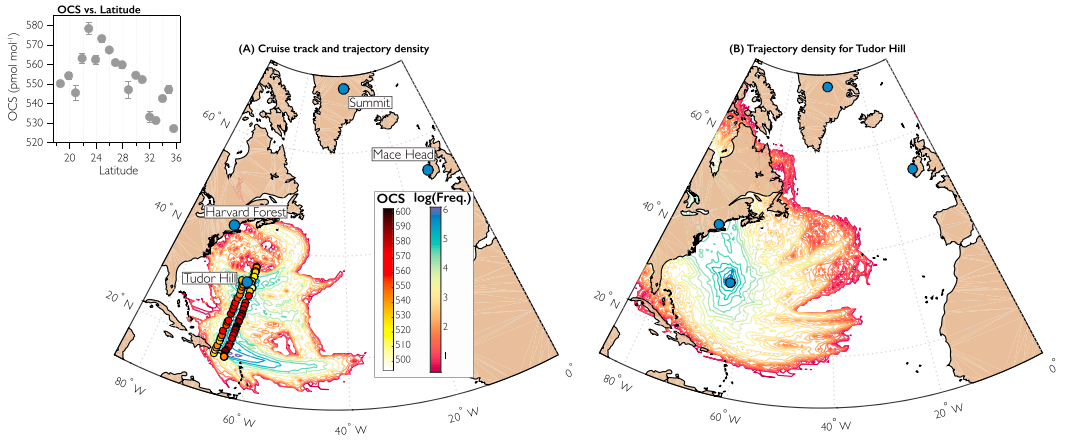

Figure 1. (a) BVAL 49 Cruise track with a slight longitudinal offset so Legs 1 (southerly) and 2 (northerly) can both be seen. The 6-hourly OCS concentrations are shown as colored points along the cruise track. The data as a time series are shown in supporting information Figure S3. The contours represent a density map of the 72 h air mass trajectory analysis along the cruise. NOAA GMD flask sites that are discussed in the text are shown. Relationship between OCS concentration and latitude is shown for the cruise data. Data were placed onto 1° latitudinal bins, and the error bars are the standard error for that bin. (b) A density map of the air mass trajectories during the Tudor Hill Observatory (TH) deployment with the same scale as Figure 1a.

≤400 to ≥800 pmol mol^{-1} [*Von Hobe et al.*, 1999; *Ulshöfer et al.*, 1995; *Commane et al.*, 2013]. Upper end values may, however, represent localized sources observed near coastlines. Spatially, the concentrations follow a latitudinal gradient (Figure 1), which was first observed from shipboard measurements [*Xu et al.*, 2001; *Weiss et al.*, 1995; *Johnson and Harrison*, 1986] and has since been observed from space, surface measurements and aboard airborne platforms [*Kuai et al.*, 2015; *Glatthor et al.*, 2015; *Montzka et al.*, 2007; *Krysztofiak et al.*, 2015]. To a first order, the latitudinal gradient is thought to reflect the regional marine OCS flux (i.e., F_{OCS}), with a strong tropical source leading to elevated concentrations at low latitudes. Less is known about the temporal variability in the marine boundary layer as most available data are from discrete measurements taken along cruise tracks [*Xu et al.*, 2001; *Mihalopoulos et al.*, 1992]. The exception would be multiyear flask records from NOAA Global Monitoring Division (GMD) taken at coastal or island sites such as Cape Kumukahi [*Montzka et al.*, 2007]. However, the low frequency of sampling at these sites precludes the study of certain dynamics.

The best constraints on the processes that drive variability of marine boundary layer OCS concentrations may come from diurnal measurements during open ocean cruises [e.g., *Von Hobe et al.*, 1999; *Uher and Andreae*, 1997]. These data indicate a diurnal cycle that is in phase with the well-documented diurnal variability in dissolved marine OCS concentrations [*Cutter et al.*, 2004; *Uher and Andreae*, 1996; *Xu et al.*, 2001] though with a considerably smaller amplitude [*Andreae and Ferek*, 1992]. However, as noted by *Von Hobe et al.* [1999], variability in marine boundary layer concentrations principally reflects air mass origins. Thus, local changes in marine production or temperature (that would influence hydrolysis and production) tend to have a significantly weaker influence on local atmospheric OCS concentrations than synoptic changes in wind direction and speed. The high sensitivity of OCS concentration to air mass origin is the result of the relatively long residence time of this gas, which leads to significant "memory" of an air mass. Therefore, marine boundary layer concentrations could be strongly influenced by changes in far afield terrestrial vegetation (a sink) [*Commane et al.*, 2013] and appear to be decoupled from local marine OCS production rates [*Von Hobe et al.*, 1999]. Thus, while marine boundary layer concentrations should approach equilibrium with the surface ocean (i.e., equation (1)), the presence of both steep latitudinal and terrestrial-marine gradients could temporarily generate significant differences between the atmospheric and oceanic concentrations under changing wind direction. This, in turn, would produce large transient marine fluxes or temporary source-to-sink (or vice versa) transitions.

The nature of atmospheric variability of OCS over the ocean has received only minor interest in the literature because it is not critical for first-order budget closure [*Kettle et al.*, 2002; *Berry et al.*, 2013; *Launois et al.*, 2015]. However, as demands for better regional OCS budgets emerge and interest in understanding the processes that drive variability at subseasonal time scales grows [*Commane et al.*, 2015], this issue requires new consideration. Here we present marine boundary layer OCS concentrations from the North Atlantic during the

fall and winter of 2014 and 2015 using a combination of continuous in situ research vessel data (Bermuda to Puerto Rico and back) followed by an extended campaign from a fixed tower at the Tudor Hill Observatory in Bermuda (TH). We present an analysis of the processes driving temporal variability in the OCS concentrations, with an emphasis on how synoptic shifts between subtropical (600 pmol mol^{-1}) and midlatitude air masses (450–500 pmol mol^{-1}) produce large differences between the marine and atmospheric concentrations and, therefore, the marine OCS flux. Lastly, we discuss how changes in atmosphere circulation could impose shifts in the marine flux and how the strength of the terrestrial sink could influence the magnitude of the net marine source.

2. Materials and Methods

2.1. Instrument

All OCS measurements were made using a Los Gatos Research, Enhanced Performance OCS analyzer (PN: 914-0028). Basic details on the instrument were previously described in *Berkelhammer et al.* [2014], but the analyzer utilized here has been improved in a number of ways including the addition of greater temperature control of the optical cavity. This modification, coupled with the fact that all measurements presented here were done in temperature-controlled labs, minimized the previously discussed temperature effects on the spectroscopy. The system operated at a cavity temperature of ~40.0°C and a pressure of ~59.0 Torr with a flow rate through the cavity of 0.7 L min^{-1}. The instrument was calibrated by the manufacturer using a permeation oven and was subsequently calibrated against a NOAA GMD reference standard (314.1 pmol mol^{-1}). The calibration of the instrument to the international standard is based on this single-point analysis, which was done using a series of extended (1–2 h) analyses of the reference gas, which was stored in a pressurized Aculife®-treated cylinder.

The NOAA reference gas was measured against compressed air samples to generate secondary standards that were generated by filling multiple 3785 cm^3 stainless steel cylinders with SilcoNert linings [*Whelan et al.*, 2013] to a pressure of 12,410 kPa (1800 psi) using an air compressor at a scuba shop. By filling cylinders at a scuba shop, there is an inherent uncertainty in the concentration of OCS that will be produced. There are filters within the compressors that tend to remove OCS and may lead to concentrations well below ambient. In other instances, contaminants in the compressor may produce secondary standards with concentrations of OCS that are elevated with respect to ambient atmosphere. We do not assume nor rely on the fact that air produced from these compressors yield identical OCS concentrations but simply measure each cylinder against the known primary reference to estimate its concentration. For this experiment, the compressors yielded secondary standards ranging from 74.0 pmol mol^{-1} to 463.0 pmol mol^{-1} (supporting information Figure S1). These reference gases were measured periodically for 10 min intervals throughout the experiment to assess both instrument drift and changes in instrument precision. We assume that OCS concentrations in the stainless steel tanks were stable over the course of the campaign, which was supported by the absence of any significant drift in their measured concentrations. This is in contrast to our previous results using calibration gases stored in uncoated aluminum cylinders, which showed significant off-gassing of OCS when pressure in the tank dropped below 6894 kPa (1000 psi) [*Berkelhammer et al.*, 2014]. In other uncoated aluminum cylinders (Luxfor cylinders used at NOAA), it is typical to observe significant losses of OCS. Based on all 10 min averages of the secondary standards, we report a standard deviation of 12.7 pmol mol^{-1} (supporting information Figure S1), which is slightly higher than the minimum uncertainty of 10.0 pmol mol^{-1} (using a 138 s integration time) reported by *Stimler et al.* [2010] for a different commercial laser spectrometer (Aerodyne Research Inc.). No measurable difference in the precision was observed between the high and low concentration standards (supporting information Figure S1).

While it is not a significant part of the analysis, we also present CO concentrations, which were generated simultaneously with OCS. At TH, these measurements were done alongside weekly NOAA GMD flask measurements [*Novelli et al.*, 1998]. Through a comparison between paired laser and flask CO, we estimate a root mean square error of 4.5 nmol mol^{-1} and a linear response of the laser analyzer across the range of 110–160 nmol mol^{-1} seen through the period of the campaign when flask and laser samples could be paired (supporting information Figure S2).

2.2. Cruise

The OCS analyzer was installed in a temperature-controlled lab on the Bermuda Institute of Ocean Sciences (BIOS) R/V *Atlantic Explorer* [e.g., *Bates et al.*, 2012]. A single 45 m long 0.635 cm (0.25 inch) OD stainless steel line was run from the ship's lab to the top of a 10 m mast at the bow of the ship. A 2 μm filter and cylindrical housing

were used to minimize rain, dust, and sea salt from entering the air lines, and a 0.159 cm (0.0625 inch) orifice was used to restrict flow and reduce pressure in the sample line. This latter feature was included to reduce the risk of condensation in the lines. The sampling line was continuously pumped at a rate of 5 l min^{-1} using a KNF Laboport pump, which was downstream of the air going into the analyzer to avoid any contaminants associated with the pump. The pump was added to minimize stagnant air in the lines. Near the instrument, the sampling line was split between the OCS analyzer and a water isotope analyzer. A set of Swagelok®; ball valves enabled the lines going to the respective instruments to be isolated during instances when one of the instruments was offline. No effect on the measurements or optical cavity pressure was detected when the system was running along with the water isotope analyzer or in isolation. The system was leak tested by spraying a high-carbon dioxide (≥10,000 ppm) air stream along all tubing connections in the sampling line.

The ship left the Bermuda Institute of Ocean Sciences (32.37°N, 64.69°W) on 26 September 2014 following the standard Bermuda Atlantic Time-series Study (BATS) validation cruise track (cruise: BVAL 49). The ship headed north to 34.67°N and then reversed course heading south (Figures 1 and S3). It reached San Juan, Puerto Rico (18.47°N, 66.11°W) on 4 October 2014 and then sailed north on 6 October 2014, reaching port in Bermuda on 11 October 2014. The cruise track is shown in Figure 1 but depicted with a slight longitudinal offset so that the northerly and southerly cruise tracks can both be visualized. With the exception of two major rain storms, when the inlet valve was closed to avoid water entering the sample lines, the system ran continuously through the cruise. OCS and CO data were collected at 1 Hz frequency but were ultimately reduced to 10 min averages to minimize noise levels. Radiation, temperature (air and ocean), wind direction and speed, and humidity were all measured as part of the standard instrumentation on the R/V *Atlantic Explorer*. We utilize the wind speed and direction to remove all data during periods when the relative wind direction was moving from stern to bow. These periods were notable from the CO data but were not associated with anomalous OCS concentrations.

2.3. Tudor Hill Observatory

Following the cruise, the instrument was moved to the Tudor Hill Marine Atmospheric Observatory (32.27°N, 64.88°W). This site is part of the NOAA GMD network and includes in situ measurements of ozone, flask measurements of molecular hydrogen and numerous carbon cycle gases (including CO), and basic meteorology. Unlike the other NOAA GMD sites discussed in section 2.6, flask OCS measurements were not made at TH. For the purposes of this study, a single 0.635 cm (0.25 inch) OD stainless steel tube was run from the temperature-controlled instrument container to the top of the 23 m tower. As with the cruise, a filter was installed at the inlet and air was pumped through the line at 5 l min^{-1}. Shortly following the deployment at the site, the tower was destroyed by Hurricane Gonzalo. After power was restored, a 10 m tower was built alongside the instrument trailer and the measurements resumed. We report data from 27 November 2014 to 22 March 2015 except for a brief period in January 2015 when power was lost to the instrument (Figure 2). As with the cruise, the raw 1 Hz data were reduced to 10 min averages and data from the wind sector of 315–210° were removed in order to minimize the effects from air traveling directly over the island. Wind from this sector typically had slightly elevated CO levels, but OCS did not appear affected by local wind fields. The effect of local terrestrial vegetation is assumed to be small because Bermuda is only 53 km^2 and these measurements were done in the winter when leaf area index at the grid cell nearest to the observatory was low (≤2) [*Xiao et al.*, 2014]. Further, the observatory is on the western end of the island, and prevailing winds are westerly from November to March. For more information on the site climatology and description of the installation see *Steen-Larsen et al.* [2014].

2.4. Trajectory Analysis

To understand how air mass origin influenced the observed OCS concentrations, back trajectories were calculated every 6 h during both the cruise and Tudor Hill campaigns. We use the Hybrid Single Particle Lagrangian Integrated Trajectory Model (HYSPLIT) [*Draxler and Rolph*, 2003] coupled to archived 1° Global Data Assimilation System (GDAS) weather simulations to generate probabilistic estimates of the pathway each air mass took to arrive at the inlet. We used an ensemble approach where 27 trajectories were modeled for each time step, and each one was initialized from a slightly modified horizontal and vertical position. Specifically, each ensemble included trajectories launched from the 1° grid cell adjacent to the starting location and from 100 m above and below each of those grid cells (i.e., a 3^3 cube). From this population of trajectories, only latitude, longitude, and time pairs were kept when the air mass was within the GDAS-modeled boundary layer. Using the trajectory ensembles, 6-hourly air mass origin probability maps were generated. These maps were then combined with Moderate Resolution Imaging Spectroradiometer (MODIS)-derived sea surface temperature

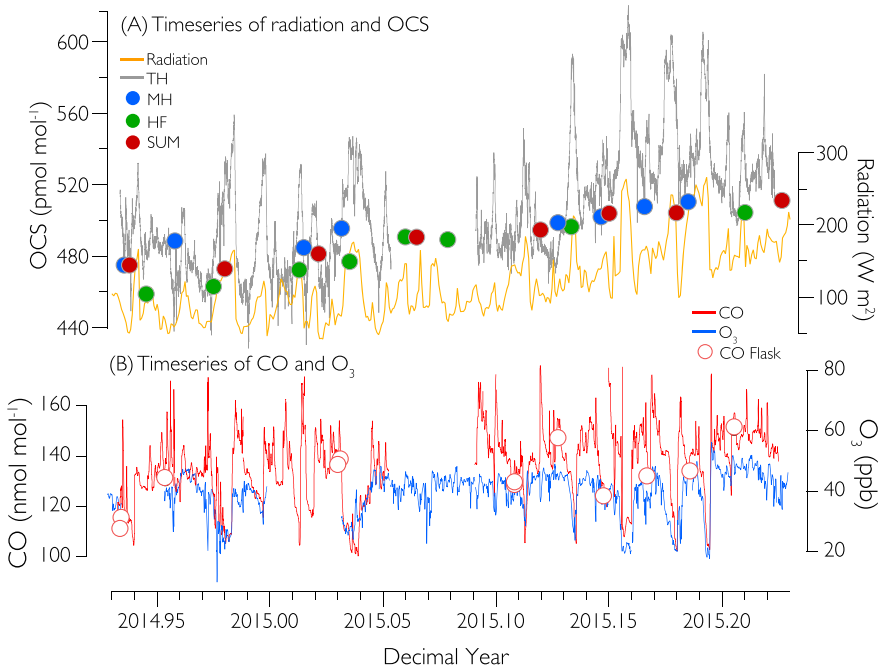

Figure 2. (a) Time series of 10 min averaged OCS from TH (gray) along with NOAA GMD flask measurements from sites shown in Figure 1. Average radiation associated with the ensemble of trajectories calculated from the Global Data Assimilation System (GDAS) forecast system every 6 h during the deployment. Radiation is averaged (i.e., includes both day and night data). Uncertainty for the 10 min averages is 12.7 pmol mol^{-1} based on repeat analysis of a reference gas (supporting information Figure S1). (b) Time series of laser-based (red line) and flask (red circle) CO and O_3 (blue line) *Novelli et al.*, 1998. Synchronous sharp changes in CO and O_3 mark transitions between southerly (maritime) and westerly (continental) air masses.

(SST) and chlorophyll concentrations to calculate the weighted average of SST and surface chlorophyll that each air parcel was exposed to before reaching the instrument (Figure 3). We used the 0.05° MODIS products [*Kilpatrick et al.*, 2015; *Ahmad et al.*, 2010], but with the resolution reduced to 1° for consistency with the GDAS data used to model the trajectories. Because data were often missing from the daily MODIS fields, 5 day averages were generated and trajectory maps projected onto this.

2.5. OCS Production Model

An analysis of direct OCS production along each trajectory was done by estimating photoproduction (equation (2)), dark production (equation (3)), and hydrolysis (equation (4)) following the approach of *Launois et al.* [2015]:

$$\text{Photo} = k \cdot \alpha_{350} \cdot \text{UV} \tag{2}$$

$$\text{Dark} = \alpha_{350} \cdot e^{55.8 - \frac{16{,}200}{T}} \tag{3}$$

$$\text{Hydrolysis} = e^{24.3 - \frac{10{,}450}{T}} + \frac{K_w}{[H^+]} \cdot e^{22.8 - \frac{6040}{T}} \tag{4}$$

where k is a quantum yield term (~2.1 fmol L^{-1}s^{-1}W^{-1}m^3); α_{350} refers to the 350 nm UV absorption coefficient (a proxy for CDOM), which was derived from the chlorophyll concentrations; UV was estimated to be 4.4% of the total irradiance [*Launois et al.*, 2015] taken from the GDAS weather fields; sea surface temperature was taken from the MODIS retrievals; and we assume a constant pH. We do not directly model the flux, which would require a 3-D model, but rather simply consider the ocean production and consumption rates at each grid cell and weight them according to the corresponding trajectory probability map. The purpose of this modeling was not to try and reproduce the observations, as we did not consider indirect OCS sources, but to test first-order controls on the factors that drive boundary layer variability.

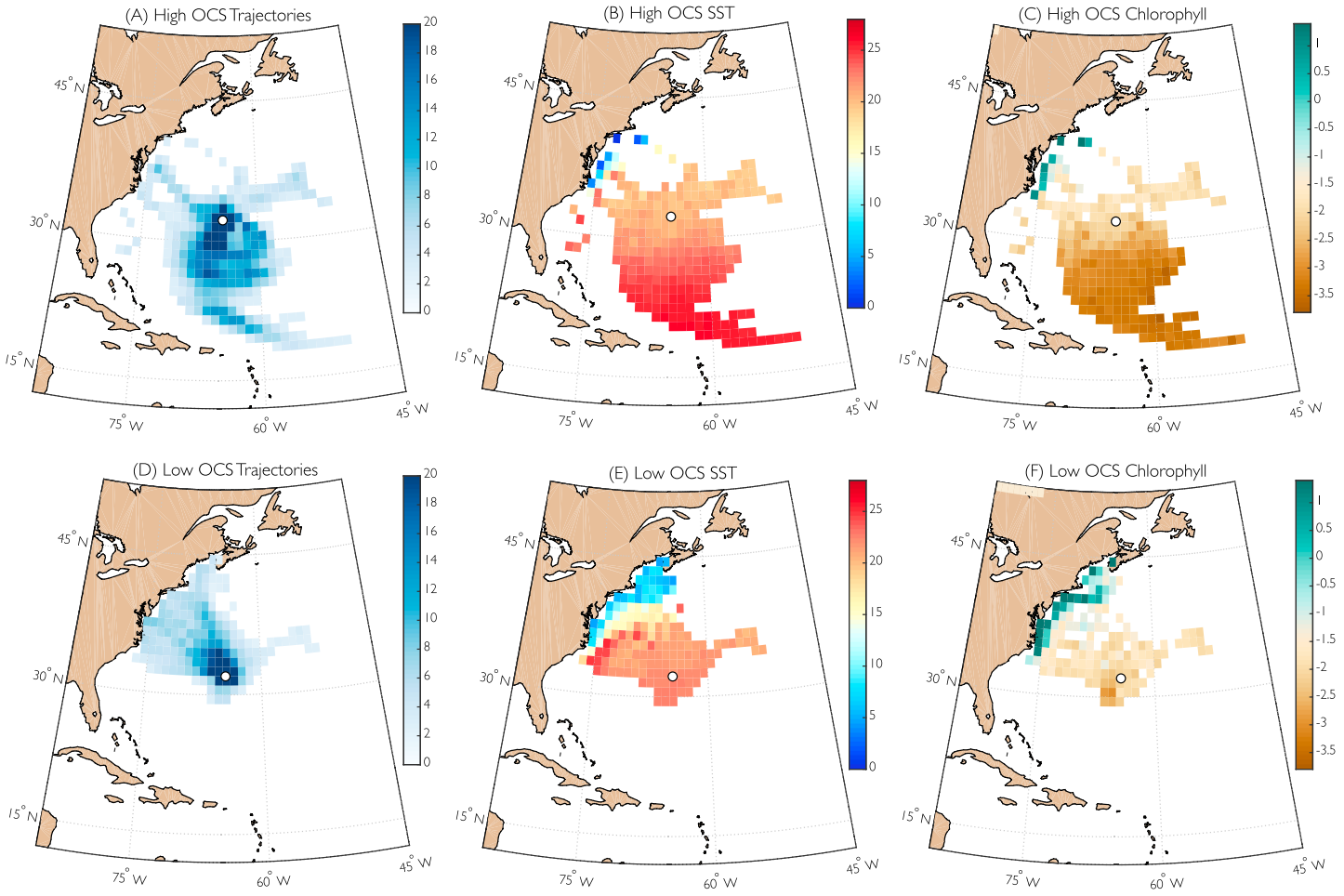

Figure 3. (a) Trajectory density, (b) SST in °C, and (c) chlorophyll in log(mg m^{-3}) during the high OCS (meridional) periods observable in Figure 2. (d–f) Same as Figures 3a–3c but showing the data during the low OCS (zonal) periods. The data were placed onto 1° grids, and all data for SST and chlorophyll were averaged for each grid cell. The location of the Tudor Hill Observatory is shown as a white dot. The corresponding wind fields for the meridional and zonal modes are shown in Figure 4.

2.6. Additional Data

NOAA GMD flask data from Harvard Forest (HF) updated from *Montzka et al.* [2007] were compared against the measurements from the Tudor Hill Observatory (TH) (locations shown in Figure 1) by scanning all trajectories from TH to identify periods when air masses passed within 500 km of HF (Figure 5). In instances where air masses arriving at TH originated from within the HF sector, we averaged the 10 min OCS concentrations at TH to a daily time scale and applied a 24 h offset to account for the average travel time of air parcels connecting the two sites. The flask data at HF is a snapshot amidst high-amplitude diurnal and synoptic variability [*Commane et al.*, 2015], and in order to assess the scale of this variability, we calculated the average difference

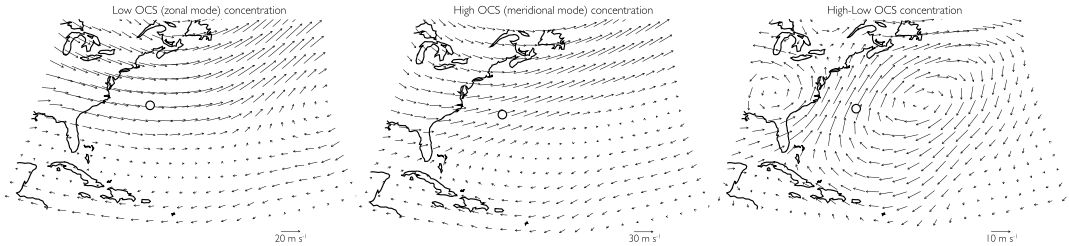

Figure 4. Average wind fields from the NCEP reanalysis [*Kalnay et al.*, 1996] data set for the periods of high (meridional mode) and low (zonal mode) OCS concentrations from Figure 3.

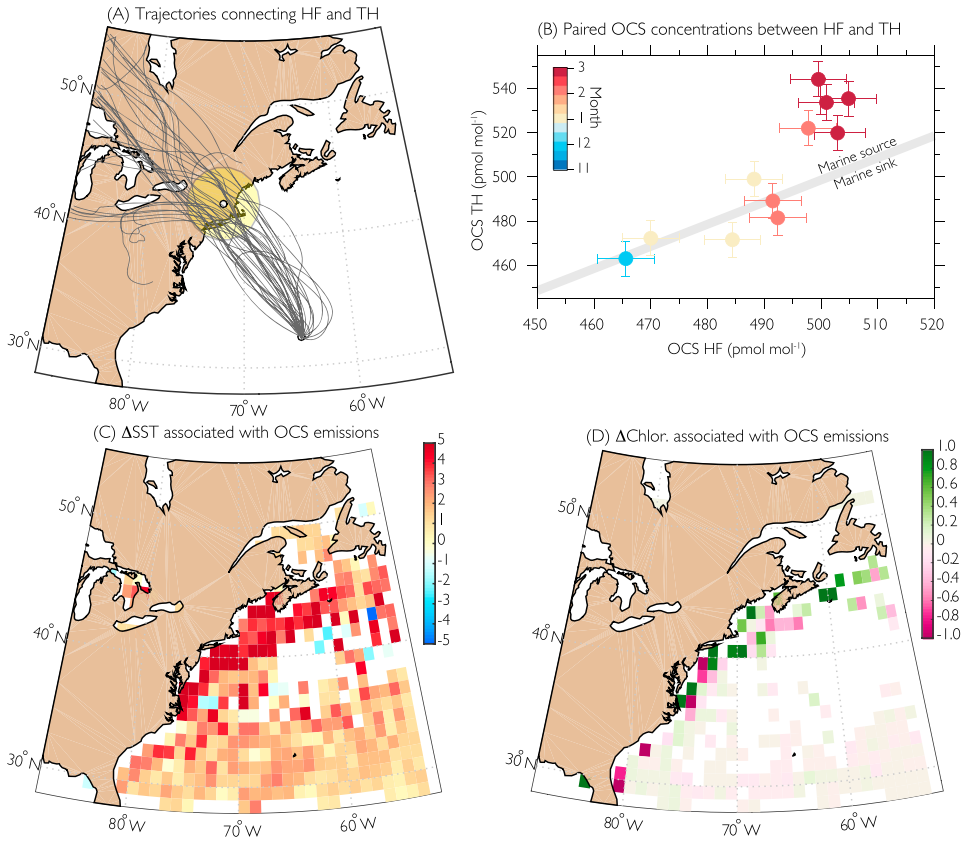

Figure 5. (a) Trajectories connecting HF and TH during the measurement campaign with the yellow circle showing the region around HF that trajectories were accepted from within. (b) The fit between daily averaged OCS at TH and the single flask measurement at HF. Error bars for TH are the standard deviation of the 10 min average over the day, and error bars for HF are the average absolute difference between weekly flask measurements at HF [*Montzka et al.*, 2007]. The line is the 1:1 fit such that data on this line are indicative of periods where there was no net emission (or uptake) along the trajectory and data above this line are associated with a net marine source. (c) The difference in SST fields between the periods with OCS emissions and no net emissions. (d) Same as in Figure 5c except for chlorophyll.

between one flask measurement and the one immediately prior and following (a week before and after) to estimate variability arising from synoptic effects. Using the December through March data from HF going back to 2001, the average absolute difference between a flask measurement and the adjacent measurements is 13.1 pmol mol^{-1}. We use this value, as opposed to the smaller analytical uncertainty, to capture a likely range of OCS concentrations that are represented from a single flask pair mean measured at HF. It is assumed that a reduction (increase) in OCS between HF and TH is associated with a marine sink (source) over the region in the North Atlantic between HF and TH.

3. Results

3.1. Cruise Data

The maximum OCS concentration observed along the cruise was 613 pmol mol^{-1} at 22.6°N, and the lowest concentration was 479 pmol mol^{-1} when the ship was in port at San Juan (18.5°N) (Figures 1 and S3). The low values observed in port and the day prior reversed an otherwise inverse latitudinal OCS gradient. We attribute the decline in OCS concentrations to reflect a terrestrial influence on the air masses, which emerged near Puerto Rico. For reference, the island of Puerto Rico has an area of 9104 km^2 compared with 53 km^2 for Bermuda. Both legs of the cruise had relatively similar OCS patterns with overall slightly higher concentrations during the first leg of the cruise, reflecting either seasonal changes or shifts in the prevailing wind directions (Figure 1). The concentrations were generally consistent with those observed in this region by *Xu et al.* [2001] during May 1998 (490–620 pmol mol^{-1}) but are higher than those authors observed during November 1997 (420–500 pmol mol^{-1}). Given the strong synoptic variability and spatial heterogeneity, these comparisons would not necessarily be expected to yield comparable values.

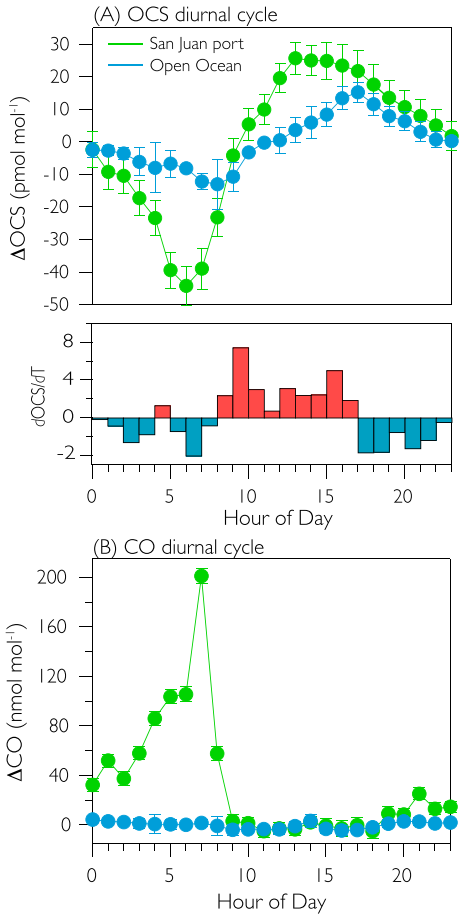

Figure 6. Average diurnal cycle of (a) OCS and (b) CO during the cruise for both open ocean (blue, 3 day average) and when the ship was in port at San Juan (2 day average). The error bars are the standard error of the repeated diurnal cycle, not the analytical uncertainty of the instrument. Both the CO and OCS are shown as anomalies relative to the average concentration of the day except for CO at San Juan which is shown relative to the evening average as this was taken to be a more representative marine value. Figure 6a (bottom) shows the rate of change of OCS for the open ocean diurnal cycle (blue line in Figure 6a, top).

During the early part of the cruise, the ship was under the predominant influence of zonal winds arriving from North America and OCS concentrations were relatively low (Figure 1). For much of the cruise, when the ship was between the influence of the westerlies and trade winds, air parcels generally remained within close distances of the ship throughout the 72 h trajectory simulations. These data are thus associated almost exclusively with local marine air masses. During this period, a measurable diurnal cycle in OCS concentrations emerged with a trough to peak difference of ~30 pmol mol^{-1} based on the average of three diurnal cycles from this period (Figure 6). The concentration peaks in the early evening (17:00 local time), multiple hours after the maximum in solar radiation. The rate of change of OCS (i.e., $\frac{dOCS}{dT}$) in the boundary layer is largest between 11:00 and 16:00 (Figure 6) and is therefore more consistent with a process driven by radiation as opposed to SST, which peaks later in the day [*Merchant et al.*, 2014]. The rate of change in OCS, however, does not follow a clear diurnal pattern and suggests the presence of midday suppression. This result shows that there are processes that disrupt a rapid and immediate response of OCS concentrations to radiation. For example, it has previously been observed that dissolved OCS concentrations, despite being largely driven by the UV flux, lag behind radiation due to the indirect biogeochemical pathways between productivity and OCS production [*Cutter et al.*, 2004; *Flöck et al.*, 1997]. Furthermore, diurnal variations in the concentrations may not only reflect the production versus hydrolysis balance but also changes in the boundary layer height. The midday deepening of the boundary layer would tend to reduce (increase) the surface concentration when free tropospheric OCS concentrations are lower (higher) than those in the boundary layer. Alternatively, if production was held constant but the boundary layer height was reduced, this would drive an increase in atmospheric concentrations unrelated to a change in marine production rates. Notably, the minimum concentration occurs a few hours after sunrise (6:45) and likely reflects the lag between the morning increase in photoproduction and deepening of the boundary layer. However, the diurnal variability observed here, which is in phase with the diurnal variation in dissolved OCS [*Cutter et al.*, 2004; *Xu et al.*, 2001], suggests that boundary layer height is not the primary determinant of the OCS concentrations. This is in contrast to terrestrial OCS observations where the maximum in boundary layer concentrations occurs in the middle of the day despite this being the period with the largest sink strength [*Berkelhammer et al.*, 2014].

As the cruise traveled south of 25°N, the air masses were associated with the trade winds and the OCS concentrations reached their maximum. As noted earlier, terrestrial influences were predominant as the ship approached Puerto Rico. This effect generated a large diurnal cycle of 80 pmol mol^{-1} as the circulation patterns shifted between sea and land breezes (Figure 6). The afternoon to nighttime (17:00 to 23:00) decline in OCS concentrations was similar to that observed in the open ocean (Figure 6), and because CO concentrations remain low until after 23:00, we conclude that this decline reflects hydrolysis and reduced photoproduction

rates as opposed to a shift from sea to land breeze. The diurnal cycles observed for the open ocean data and from port begin to diverge after midnight, coincident with the rise in CO near Puerto Rico.

3.2. Tower Data

The initial concentrations measured at TH were ~500 pmol mol^{-1}, similar to the marine boundary layer values measured as the cruise approached Bermuda (Figures 1 and 2). Through the deployment at TH, the concentrations were characterized by strong synoptic variability, ranging between 440 and 540 pmol mol^{-1} during November and December and steadily rising to concentrations between 500 and 600 pmol mol^{-1} in February and March (Figure 2). A comparison of the TH data with flask data from sites at higher latitudes in the North Atlantic show that during one type of synoptic mode (*zonal mode*), there is similarity across all sites and a consistency in the amplitude and timing of the seasonal cycle (Figure 2). This occurs when the jet stream was south of Bermuda so that air masses reaching the site had midlatitude characteristics (Figure 4). However, during the second synoptic mode (*meridional mode*), concentrations were significantly greater at TH relative to the higher-latitude sites (Figure 2). The high values seen during the meridional mode are similar to the maximum concentrations observed from the research vessel (Figure 1). This less frequent mode occurs when northerly migration of the jet stream leads to TH being strongly influenced by subtropical and tropical air masses bringing high OCS concentrations farther north (Figure 4). These modes are generally well captured by both the CO and O_3 data from TH and indicate a distinction in the chemical composition of subtropical maritime and midlatitude continental air masses. Trajectory maps averaged from the two different synoptic modes reveal that high OCS values were associated with southerly flow where air had reached TH after passing over warm SSTs (≥25°C) and water with relatively low chlorophyll concentrations (Figure 3). Periods of low OCS concentrations were associated with northwesterly wind patterns (coincidentally passing nearby the HF site, Figure 5), where air masses had interacted with cooler and more productive coastal waters off the continental U.S. (Figure 3).

Using the trajectory simulations, we identified a small number of instances when air reaching TH from nearby HF occurred coincident with a NOAA GMD flask measurement (Figure 5). From November until early February, the concentration of OCS was virtually unchanged as air masses traveled between HF and TH. There may have been uptake and emissions of OCS along the pathway, but there was no net cumulative marine flux. Beginning in late February and continuing until the end of the campaign, we saw an increase in OCS concentrations between HF and TH, which is indicative of a net oceanic source. Because the analysis required the presence of specific wind fields that connected HF and TH sites, the source and sink analysis is discontinuous but points toward a seasonal transition from no net flux in the winter to a source beginning in the spring. The presence of this transition and its timing is roughly consistent with the broad patterns of the North Atlantic flux direction observed in both modeling and earlier shipboard analyses [*Launois et al.*, 2015; *Preiswerk and Najjar*, 2000; *Ulshöfer et al.*, 1995; *Von Hobe et al.*, 1999]. A comparison of the SST and chlorophyll fields associated with the time periods of either no OCS flux or a source reveal a significant difference in SSTs (following the seasonal trend) but no apparent difference in chlorophyll concentrations. The higher SSTs during periods when there was an OCS source was not necessarily causal. Higher SSTs would increase hydrolysis rates (a sink); however, higher SSTs are also associated with higher radiation and therefore increased photoproduction of not only OCS but also DMS and CS_2.

3.3. Model of Boundary Layer OCS

A regression model between OCS concentration and radiation, where radiation is defined as the total radiation flux reaching the surface over the 72 h trajectory, indicates a strong linear relationship between the two that is continuous across the TH and cruise data sets (Figure 7). When the linear fit to only the TH data is extended across the range of the cruise data, it encompasses over 90% of the cruise OCS concentration measurements, suggesting that a single linear model is effective to describe the entire data set. However, we note that radiation and OCS from only the cruise data are not related with statistical significance. One interpretation is that the sensitivity of OCS to radiation is reduced at the very high levels of radiation encountered by the air masses sampled from the cruise. However, the cruise data set is small and encompasses only a limited radiation range relative to the TH data set, making it difficult to confidently assess whether the sensitivity of OCS to high levels of radiation was weaker. Radiation and SST were related to one another, and thus, SST and OCS were also correlated. However, unlike the linear response to radiation, there is only a weak sensitivity of OCS to SST below a threshold of 20°C.

The OCS correlation with chlorophyll is weakly negative but not significant and is the result of an inverse correlation between radiation and chlorophyll (supporting information Figure S5). Although this analysis suggests

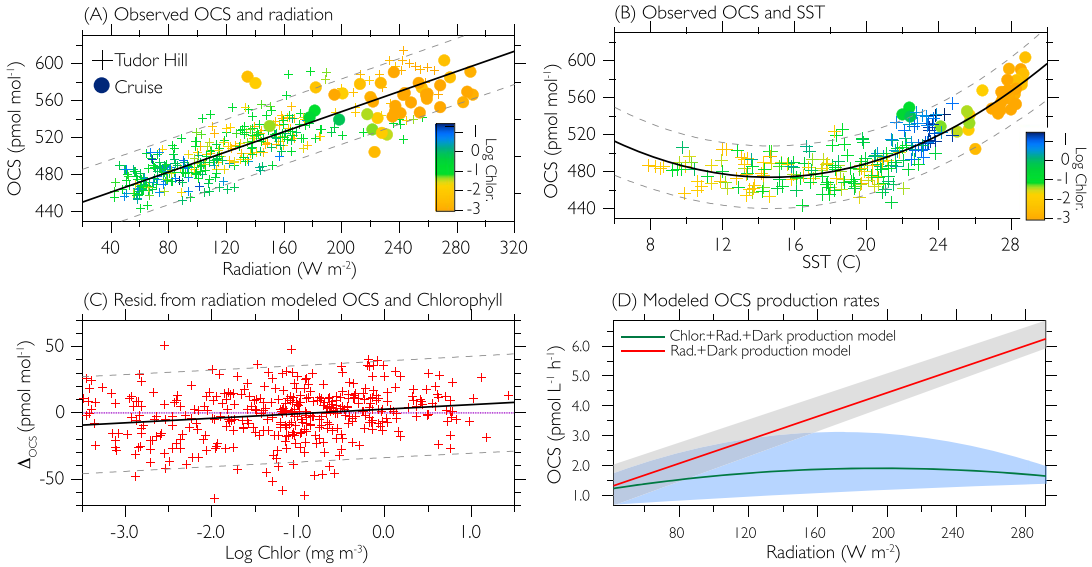

Figure 7. (a) Relationship between radiation and OCS for the cruise and TH data. Radiation is the average from the trajectory maps, and the markers are colored with chlorophyll. The line is the best fit linear regression based on the TH data with the error bars capturing the 95% prediction band for this fit using a Monte Carlo simulation. (b) Relationship between SST and OCS for the cruise and TH data. SST is the average from the trajectory maps, and the markers are colored with chlorophyll as in Figure 7a. The line is the best fit second-order polynomial regression using the TH data with the error bars capturing the 95% prediction band for this fit. (c) The fit between the residual of the linear model of OCS and radiation (Figure 7a) and corresponding chlorophyll (*x* axis). The purple line is the zero residual, and the black line is the fit to the data, whose slope is not significantly different from zero. If chlorophyll concentration limited the effect of radiation on OCS, we would anticipate negative (positive) residuals to occur when chlorophyll concentrations were low (high). (d) Modeled OCS production rates against radiation using a model that both includes (red) and excludes (green) the influence of chlorophyll (CDOM) on photoproduction rates. Error bars are the 10th and 90th percentiles of the simulations.

that chlorophyll is not a first-order determinant of OCS concentrations, it may be that chlorophyll modulates the sensitivity of OCS to radiation. We tested this by comparing the residual between the linear fit of radiation and OCS against chlorophyll concentrations. If this analysis yielded a positive correlation, it would imply that OCS concentrations falling below (above) the expected response of OCS to radiation were the result of low (high) chlorophyll concentrations (Figure 7). We found a weak but insignificant positive correlation between the residual of the radiation model and chlorophyll, suggesting that there was no apparent threshold at which chlorophyll concentration significantly modulated the radiation control on OCS.

We assessed the OCS production rates for each trajectory map with a pair of models that either included or excluded chlorophyll as a limiting factor for photoproduction (equation (2)). All additional terms including hydrolysis (equation (4)) and dark production (equation (3)) were included, both of which were related to chlorophyll and indirectly to radiation through the effect on temperature. These simulations were not intended to reproduce the OCS concentration measurements but to identify the dominant processes driving boundary layer concentrations. The most effective model was one that excluded chlorophyll and simply used a quantum yield term multiplied by radiation [*Andreae and Ferek*, 1992]. When chlorophyll is included in the model for photoproduction, it resulted in a weak and nonlinear relationship between the OCS flux and radiation. This result emerged from the presence of an inverse relationship between radiation and chlorophyll such that periods with the highest radiation flux were coincident with the lowest chlorophyll concentrations (supporting information Figure S5). This is not indicative of an ocean-wide relationship but emerges in this data set because subtropical waters associated with high radiation (and high boundary layer OCS concentrations) had low chlorophyll concentrations, whereas the trajectories associated with low radiation were associated with the most productive waters. As a consequence, the effect of radiation and chlorophyll on OCS production cancel one another out and lead to modeled OCS fluxes that are highest during periods of both average radiation flux and chlorophyll concentrations.

We do not include indirect emissions of DMS and CS_2 in this model owing to a lack of constraints, but these fluxes are likely important in setting the response of boundary layer OCS to forcing including radiation and chlorophyll. For example, *Levine et al.* [2015] notes a negative correlation between DMS and chlorophyll associated with biological consumption of DMS. Therefore, a decrease in chlorophyll could increase the DMS flux

and consequently OCS concentrations through oxidation. This provides an alternative explanation of the negative response of OCS concentrations to chlorophyll. However, DMS concentration in the waters near TH are very low in the winter, and thus we do not anticipate that the shifts in OCS observed at TH are associated with the variability in local DMS production [*Levine et al.*, 2015]. A simpler explanation is that the indirect emissions are supporting the observed relationship between OCS and radiation. The linear correlation we observed between OCS and radiation is similar in form to that observed from a global analysis of dissolved DMS concentrations and radiation from *Vallina and Simó* [2007]. If it is assumed that the molar conversion rate between DMS and OCS is rapid and constant, then this would change the slope of the linear function but not its form. Similarly, CS_2 fluxes are positively correlated with radiation [*Chin and Davis*, 1993] and temperature [*Xie and Moore*, 1999] (supporting information Figure S4), and this, again, could shift the slope of the function but not disrupt the presence of a strong correlation between OCS concentration and radiation. However, depending on the time constants for the conversion of indirect precursors to OCS, this could generate temporary nonlinear characteristics of the response function even if the direct and indirect sources all have linear response functions.

4. Discussion

The shipboard and tower data presented here (Figures 1 and 2) suggest that the OCS variations we observed in the marine boundary layer can be explained primarily as a linear function of an air mass' radiation and latitudinal history (Figure 7). We anticipated that chlorophyll (a proxy for CDOM) would have had a significant influence on the OCS concentrations, but this was not borne out with the data. In fact, by considering chlorophyll as an explanatory variable, boundary layer OCS had a weak and nonmonotonic relationship with radiation (Figure 7). The simplest explanation is that radiation is the dominant limiting factor for OCS production in the North Atlantic during the fall and winter. This suggests that even under conditions of low CDOM, there is sufficient dissolved organic sulfur to support radiation-limited direct or indirect OCS emissions. Another possible mechanism to explain the lack of a chlorophyll limitation on OCS emissions could be an inverse relationship between DMS and chlorophyll, which would lead to indirect OCS emissions that are anticorrelated with chlorophyll. Although there remain uncertainties regarding the exact mechanisms driving OCS variability, the results are consistent with the idea of significant tropical marine OCS fluxes suggested by *Kuai et al.* [2015] and *Berry et al.* [2013]. This flux would be driven by the persistently high radiation despite broad areas in the low latitudes with low productivity. Earlier latitudinal transects of marine boundary layer air had also found a similar pattern [*Xu et al.*, 2001; *Johnson and Harrison*, 1986], and recent mechanistic studies of the marine OCS cycle suggest that the high concentrations over low-latitude oceans can be explained by high rates of photoproduction and hydrolysis and dark production rates that have approximately equal flux magnitudes but of the opposite sign [*Launois et al.*, 2015].

We note, however, that some earlier shipboard data (from discrete flask measurements) had not found elevated OCS concentrations at low latitudes [*Weiss et al.*, 1995]. One explanation for relatively low OCS concentrations in the boundary layer over areas of otherwise elevated OCS production is that air masses had recently passed over regions of high terrestrial productivity. For example, over the eastern tropical Pacific, air masses that had recently passed over the Amazon would be depleted in OCS [*Glatthor et al.*, 2015]. We see a small-scale example of this during the cruise when measurements were made in proximity to Puerto Rico. Under these conditions, OCS concentrations were much lower than would otherwise be expected given the high radiation flux. The nearby landmass reduced boundary layer concentrations by as much as 20% and had an observable effect over 100 km from the coast. A consistent negative relationship between CO and OCS observed in proximity to Puerto Rico confirm the terrestrial signature of these air parcels (Figure 6). The legacy of terrestrial impacts on atmospheric OCS concentrations was previously noted in comparisons between the abundance of biogenic aerosols and low OCS concentrations [*de Gouw et al.*, 2009] and was noted from shipboard measurements off the coast of California [*Commane et al.*, 2013].

Measurements from the Tudor Hill Observatory in Bermuda showed evidence for high-amplitude synoptic-scale variability that had not previously been documented for the marine boundary layer. The range of OCS variability at this site arises from the fact that Bermuda sits at a fortuitous latitude, such that it is exposed to midlatitude and subtropical air masses associated with normal variations in the jet stream. This enabled observations from a single site to track OCS concentrations across a wide latitudinal range (Figure 1). There was a clear shift in CO and O_3 associated with these circulation changes, which is a result of continental emissions

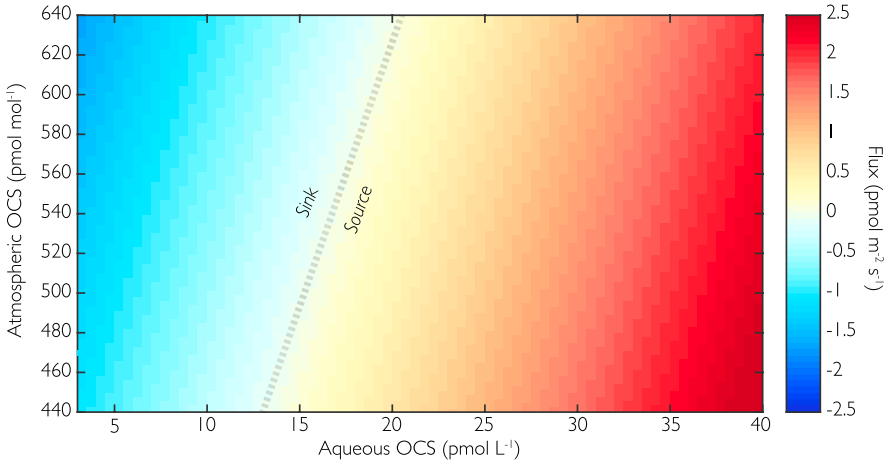

Figure 8. The relationship between atmospheric (ordinate) and aqueous (abscissa) OCS concentrations with the range for the former taken from Figures 1 and 2 and values for the latter taken from the diurnal measurements by *Cutter et al.* [2004]. Henry's law constants and piston velocity were calculated as the average over the sampling campaign.

from the northeastern United States [*Conte and Weber*, 2002]. When TH was under the influence of midlatitude air masses (zonal mode), it had OCS concentrations almost identical to those concomitantly observed as far north as Greenland (SUM in Figure 2). On the other hand, during periods when the site was under the influence of subtropical air masses (meridional mode), it had concentrations as much as 100 pmol mol^{-1} higher than those observed at the more northerly flask sites. The subtle latitudinal gradient during the zonal model is consistent with the analyses presented in *Montzka et al.* [2007], and it suggests a lack of any significant OCS sources (or sinks) in the Northern Hemisphere during the winter. Through our comparison between contemporaneous measurements at Harvard Forest and TH, we indeed find the absence of any net marine flux (source or sink) for most of the campaign [*Ulshöfer et al.*, 1995] (Figure 5).

Because of the presence of a large tropical to midlatitude OCS gradient and that the time scale for atmospheric transport is faster than the time for the ocean and atmosphere to reach equilibrium, the OCS concentration of an air mass retains a signature associated with its region of origin as opposed to the local marine production. This implies that the flux from the ocean would vary on time scales set both by marine production (diurnal and seasonal) and atmospheric transport (synoptic to seasonal). Using a range of dissolved OCS concentrations observed nearby Bermuda from *Cutter et al.* [2004] and the range of atmospheric OCS measured in the boundary layer at TH (Figure 2), we use equation (1) to test how the direct OCS flux is sensitive to synoptic variability in the atmosphere (Figure 8). The results show that the magnitude and sign of the marine flux shifts not only on diurnal time scales, a function of radiation-controlled marine production, but also on synoptic time scales, a function of changes in the atmosphere to ocean gradient. This analysis could be extended to consider how large-scale atmospheric modes such as the North Atlantic Oscillation (defined as the pressure gradient between the Icelandic Low and Azores High [*Hurrell*, 1995]) would influence the marine flux. For example, an enhanced pressure gradient would increase meridional transport of OCS. This would increase OCS concentrations over the midlatitude and polar oceans and, even with relatively stable marine OCS production rates, change the OCS flux by altering the atmosphere to aqueous gradient. The time scale under which this would be relevant would be dependent both on the strength of the atmospheric circulation and the response of the mixing depth to changes in wind speed and direction. A coupled 3-D model would be needed to test the effect this would have on the marine to atmospheric flux.

For Bermuda, we find large synoptic variability arising from changes in atmospheric circulation over the ocean but similar or even larger OCS variability might be present over coastal regions that would be sensitive to changes in adjacent terrestrial productivity (an OCS sink) [*Commane et al.*, 2013]. At these locations, an increase in terrestrial productivity would lower OCS concentrations over the adjacent ocean, increase the gradient between the marine boundary layer and dissolved OCS (assuming production rates are constant), and increase the marine flux. This would occur both with seasonal vegetation changes and also potentially over

long time scales as land use or ecosystems vary. This mechanism could act as a means to couple the marine and terrestrial OCS cycles such that increased vegetation uptake would increase the direct component of the marine OCS flux.

5. Conclusions

The use of global and regional simulations of OCS to constrain terrestrial gross primary production [*Berry et al.*, 2013] coupled with its potential to study the secular responses of terrestrial productivity to climate forcing [*Aydin et al.*, 2016] has motivated a resurgent interest in OCS. The capacity to now make both continuous high-resolution surface measurements [*Stimler et al.*, 2010] and global remotely sensed estimates of OCS [*Kuai et al.*, 2015] are yielding opportunities to constrain elements of the OCS budget that have long been uncertain. While certain applications, such as its use as an independent plot-scale gross primary production proxy [*Asaf et al.*, 2013], do not require a globally closed budget, large uncertainties in the magnitude of the ocean flux currently limit the ability to isolate the terrestrial gross primary production component of interannual OCS variability or long-term trends. Here we present continuous observations of marine boundary layer OCS over the North Atlantic and find a surprisingly simple radiation limitation on its flux. Similar studies in other regions would be needed to test whether the response of OCS to radiation is stable in space and time. We anticipate that given the mixture of indirect and direct OCS pathways that there will be variability in the slope of the response.

Previous work on the global OCS cycle has largely neglected the potential coupling between the marine and terrestrial fluxes. We suggest that because OCS concentrations over the ocean can reflect far afield changes, an increase in terrestrial uptake would lower concentrations over the ocean and lead to an offsetting increased marine flux. While the current work is not capable of fully exploring this idea, longer shipboard data sets that include both dissolved and atmospheric OCS would shed light on this effect. In addition, new global modeling efforts have the potential to test these interactions and coupling between components of the OCS cycle [*Launois et al.*, 2015; *Berry et al.*, 2013; *Suntharalingam et al.*, 2008]. Model diagnosis has relied almost exclusively on trying to match the average seasonal cycle derived from the NOAA GMD flask network, but with higher resolution data, the subseasonal features we discuss here can be used to test the mechanisms driving the timing, amplitude, and interannual variability of the seasonal cycle.

A number of recent studies have highlighted that tropical oceans are an important global source of OCS through either direct or indirect emissions [*Berry et al.*, 2013; *Kuai et al.*, 2015], and the work presented here supports this. It can be anticipated that in the presence of a persistent and high radiation input, this flux would be fairly stable on interannual time scales even amidst changes in chlorophyll concentrations. Some of the tropical OCS would be lost to the stratosphere associated with deep convection [*Kremser et al.*, 2015], whereas some would be retained in the trade wind belt and consumed by tropical vegetation [*Berry et al.*, 2013]. The loss of OCS from deep convection affects stratospheric aerosol formation and thus the global climate [*Crutzen*, 1976], whereas the loss of OCS to tropical vegetation is a major sink term in the tropospheric budget. It has been postulated, for example, that changes in global OCS concentrations over the Holocene may be associated with changes in terrestrial primary productivity, notably the tropics [*Aydin et al.*, 2016]. Here we document that OCS concentrations of air masses along meridional transport pathways retain the high concentrations from lower latitudes. The amount of meridional mixing would be sensitive to large-scale ocean-atmosphere modes that influence wave patterns in the jet stream. Ultimately, this would shift the latitudinal gradient and the average concentrations over the subtropical, midlatitude, and polar oceans and would be important in determining the magnitude and sign of the marine flux. Whether interannual changes in synoptic atmospheric modes would influence global budget terms in a substantive way is a question that can be addressed in future studies using longer high-resolution time series and coupled models that reproduce realistic atmospheric circulation patterns.

Acknowledgments

MODIS chlorophyll *a* concentrations were originally obtained from ftp://podaac-ftp.jpl.nasa.gov/ and were provided by the Integrated Climate Data Center (ICDC, http://icdc.zmaw.de) University of Hamburg, Hamburg, Germany, in netCDF format for the period September 2014 to March 2015. MODIS SST data were originally obtained from ftp://podaac-ftp.jpl.nasa.gov/ and were provided by the Integrated Climate Data Center (ICDC, http://icdc.zmaw.de) University of Hamburg, Hamburg, Germany, in netCDF format for the period September 2014 to March 2015. Operation of the BIOS Tudor Hill Marine Atmospheric Observatory is funded by NSF grant OCE-1430741. Flask OCS data were downloaded from the NOAA GMD public FTP site. All carbonyl sulfide data discussed in the text are included in supporting information Tables S1 and S2 and are freely available for use without author consent.

References

Ahmad, Z., B. Franz, C. McClain, E. Kwiatkowska, J. Werdell, E. Shettle, and B. Holben (2010), New aerosol models for the retrieval of aerosol optical thickness and normalized water-leaving radiances from the SeaWiFS and MODIS sensors over coastal regions and open oceans, *Appl. Opt.*, *49*(29), 5545–5560.

Andreae, M., and R. Ferek (1992), Photochemical production of carbonyl sulfide in seawater and its emission to the atmosphere, *Global Biogeochem. Cycles*, *6*(2), 175–183.

Asaf, D., E. Rotenberg, F. Tatarinov, U. Dicken, S. A. Montzka, and D. Yakir (2013), Ecosystem photosynthesis inferred from measurements of carbonyl sulphide flux, *Nat. Geosci.*, *6*(3), 186–190.

Aydin, M., T. Fudge, K. Verhulst, M. Nicewonger, E. Waddington, and E. Saltzman (2014), Carbonyl sulfide hydrolysis in Antarctic ice cores and an atmospheric history for the last 8000 years, *J. Geophys. Res. Atmos.*, *119*, 8500–8514, doi:10.1002/2014JD021618.

Aydin, M., J. Campbell, T. Fudge, K. Cuffey, M. Nicewonger, K. Verhulst, and E. Saltzman (2016), Changes in atmospheric carbonyl sulfide over the last 54,000 years inferred from measurements in Antarctic ice cores, *J. Geophys. Res. Atmos.*, *121*, 1943–1954, doi:10.1002/2015JD024235.

Barnes, I., K. Becker, and I. Patroescu (1994), The tropospheric oxidation of dimethyl sulfide: A new source of carbonyl sulfide, *Geophys. Res. Lett.*, *21*(22), 2389–2392.

Bates, N., M. Best, K. Neely, R. Garley, A. Dickson, and R. Johnson (2012), Detecting anthropogenic carbon dioxide uptake and ocean acidification in the North Atlantic Ocean, *Biogeosciences*, *9*(7), 2509–2522.

Berkelhammer, M., D. Asaf, C. Still, S. Montzka, D. Noone, M. Gupta, R. Provencal, H. Chen, and D. Yakir (2014), Constraining surface carbon fluxes using in situ measurements of carbonyl sulfide and carbon dioxide, *Global Biogeochem. Cycles*, *28*, 161–179, doi:10.1002/2013GB004644.

Berry, J., et al. (2013), A coupled model of the global cycles of carbonyl sulfide and CO_2: A possible new window on the carbon cycle, *J. Geophys. Res. Biogeosci.*, *118*, 842–852.

Campbell, J., et al. (2008), Photosynthetic control of atmospheric carbonyl sulfide during the growing season, *Science*, *322*(5904), 1085–1088.

Chin, M., and D. Davis (1993), Global sources and sinks of OCS and CS_2 and their distributions, *Global Biogeochem. Cycles*, *7*(2), 321–337.

Commane, R., S. Herndon, M. Zahniser, B. Lerner, J. McManus, J. Munger, D. Nelson, and S. Wofsy (2013), Carbonyl sulfide in the planetary boundary layer: Coastal and continental influences, *J. Geophys. Res. Atmos.*, *118*, 8001–8009, doi:10.1002/jgrd.50581.

Commane, R., L. K. Meredith, I. T. Baker, J. A. Berry, J. W. Munger, S. A. Montzka, P. H. Templer, M. S. Zahniser, and S. C. Wofsy (2015), Seasonal fluxes of carbonyl sulfide in a midlatitude forest, *Proc. Natl. Acad. Sci. U.S.A.*, *112*(46), 14,162–14,167.

Conte, M. H., and J. C. Weber (2002), Plant biomarkers in aerosols record isotopic discrimination of terrestrial photosynthesis, *Nature*, *417*(6889), 639–641.

Crutzen, P. (1976), The possible importance of COS for the sulfate layer of the stratosphere, *Geophys. Res. Lett.*, *3*(2), 73–76.

Cutter, G., L. Cutter, and K. Filippino (2004), Sources and cycling of carbonyl sulfide in the Sargasso Sea, *Limnol. Oceanogr.*, *49*(2), 555–565.

de Gouw, J., C. Warneke, S. Montzka, J. Holloway, D. Parrish, F. Fehsenfeld, E. Atlas, R. Weber, and F. Flocke (2009), Carbonyl sulfide as an inverse tracer for biogenic organic carbon in gas and aerosol phases, *Geophys. Res. Lett.*, *36*, L05804, doi:10.1029/2008GL036910.

Draxler, R., and G. Rolph (2003), Hysplit (Hybrid Single-Particle Lagrangian Integrated Trajectory) Model Access via NOAA ARL Ready Website, [Available at http://www.arl.noaa.gov/ready/hysplit4.html.]

Elliott, S., E. Lu, and F. S. Rowland (1989), Rates and mechanisms for the hydrolysis of carbonyl sulfide in natural waters, *Environ. Sci. Technol.*, *23*(4), 458–461.

Ferek, R., and M. Andreae (1983), The supersaturation of carbonyl sulfide in surface waters of the Pacific Ocean off Peru, *Geophys. Res. Lett.*, *10*(5), 393–396.

Flöck, O., M. Andreae, M. Dräger, and Mar. Chem. (1997), Environmentally relevant precursors of carbonyl sulfide in aquatic systems, *59*(1), 71–85.

Glatthor, N., et al. (2015), Tropical sources and sinks of carbonyl sulfide observed from space, *Geophys. Res. Lett.*, *42*, 10,082–10,090, doi:10.1002/2015GL066293.

Hurrell, J. W. (1995), Decadal trends in the North Atlantic Oscillation: Regional temperatures and precipitation, *Science*, *269*(5224), 676–679.

Johnson, J., and H. Harrison (1986), Carbonyl sulfide concentrations in the surface waters and above the Pacific Ocean, *J. Geophys. Res.*, *91*(D7), 7883–7888.

Kalnay, E., et al. (1996), The NCEP/NCAR 40-year reanalysis project, *Bull. Am. Meteorol. Soc.*, *77*(3), 437–471.

Kettle, A., U. Kuhn, M. Von Hobe, J. Kesselmeier, and M. Andreae (2002), Global budget of atmospheric carbonyl sulfide: Temporal and spatial variations of the dominant sources and sinks, *J. Geophys. Res.*, *107*(D22), 4658, doi:10.1029/2002JD002187.

Kilpatrick, K., G. Podestá, S. Walsh, E. Williams, V. Halliwell, M. Szczodrak, O. Brown, P. Minnett, and R. Evans (2015), A decade of sea surface temperature from MODIS, *Remote Sens. Environ.*, *165*, 27–41.

Kremser, S., N. B. Jones, M. Palm, B. Lejeune, Y. Wang, D. Smale, and N. M. Deutscher (2015), Positive trends in Southern Hemisphere carbonyl sulfide, *Geophys. Res. Lett.*, *42*, 9473–9480, doi:10.1002/2015GL065879.

Krysztofiak, G., Y. V. Té, V. Catoire, G. Berthet, G. C. Toon, F. Jégou, P. Jeseck, and C. Robert (2015), Carbonyl sulphide (OCS) variability with latitude in the atmosphere, *Atmos. Ocean*, *53*(1), 89–101.

Kuai, L., et al. (2015), Estimate of carbonyl sulfide tropical oceanic surface fluxes using Aura Tropospheric Emission Spectrometer observations, *J. Geophys. Res. Atmos.*, *120*, 11,012–11,023, doi:10.1002/2015JD023493.

Launois, T., S. Belviso, L. Bopp, C. Fichot, and P. Peylin (2015), A new model for the global biogeochemical cycle of carbonyl sulfide—Part 1: Assessment of direct marine emissions with an oceanic general circulation and biogeochemistry model, *Atmos. Chem. Phys.*, *14*, 20–677.

Levine, N. M., D. A. Toole, A. Neeley, N. R. Bates, S. C. Doney, and J. W. Dacey (2015), Revising upper-ocean sulfur dynamics near Bermuda: New lessons from 3 years of concentration and rate measurements, *Environ. Chem.*, *13*(2), 302–313.

Merchant, C. J., et al. (2014), Sea surface temperature datasets for climate applications from Phase 1 of the European Space Agency Climate Change Initiative (SST CCI), *Geosci. Data J.*, *1*(2), 179–191.

Mihalopoulos, N., B. Nguyen, J. Putaud, and S. Belviso (1992), The oceanic source of carbonyl sulfide (COS), *Atmos. Environ. Part A*, *26*(8), 1383–1394.

Montzka, S., M. Aydin, M. Battle, J. Butler, E. Saltzman, B. Hall, A. Clarke, D. Mondeel, and J. Elkins (2004), A 350-year atmospheric history for carbonyl sulfide inferred from Antarctic firn air and air trapped in ice, *J. Geophys. Res.*, *109*, D22302, doi:10.1029/2004JD004686.

Montzka, S., P. Calvert, B. Hall, J. Elkins, T. Conway, P. Tans, and C. Sweeney (2007), On the global distribution, seasonality, and budget of atmospheric carbonyl sulfide (COS) and some similarities to CO_2, *J. Geophys. Res.*, *112*, D09302, doi:10.1029/2006JD007665.

Novelli, P., K. Masarie, and P. Lang (1998), Distributions and recent changes of carbon monoxide in the lower troposphere, *J. Geophys. Res.*, *103*(D15), 19,015–19,033.

Preiswerk, D., and R. Najjar (2000), A global, open-ocean model of carbonyl sulfide and its air-sea flux, *Global Biogeochem. Cycles*, *14*(2), 585–598.

Sandoval-Soto, L., M. Stanimirov, M. Von Hobe, V. Schmitt, J. Valdes, A. Wild, and J. Kesselmeier (2005), Global uptake of carbonyl sulfide (COS) by terrestrial vegetation: Estimates corrected by deposition velocities normalized to the uptake of carbon dioxide (CO_2), *Biogeosciences*, *2*(2), 125–132.

Steen-Larsen, H. C., A. E. Sveinbjörnsdottir, A. J. Peters, V. Masson-Delmotte, M. P. Guishard, G. Hsiao, J. Jouzel, D. Noone, J. K. Warren, and J. W. C. White (2014), Climatic controls on water vapor deuterium excess in the marine boundary layer of the North Atlantic based on 500 days of in situ, continuous measurements, *Atmos. Chem. Phys.*, *14*(15), 7741–7756.

Stimler, K., D. Nelson, and D. Yakir (2010), High precision measurements of atmospheric concentrations and plant exchange rates of carbonyl sulfide using mid-IR quantum cascade laser, *Global Change Biol.*, *16*(9), 2496–2503.

Suntharalingam, P., A. Kettle, S. Montzka, and D. Jacob (2008), Global 3-D model analysis of the seasonal cycle of atmospheric carbonyl sulfide: Implications for terrestrial vegetation uptake, *Geophys. Res. Lett.*, *35*, L19801, doi:10.1029/2008GL034332.

Uher, G., and M. Andreae (1996), The diel cycle of carbonyl sulfide in marine surface waters: Field study results and a simple model, *Aquat. Geochem.*, *2*(4), 313–344.

Uher, G., and M. Andreae (1997), Photochemical production of carbonyl sulfide in North Sea water: A process study, *Limnol. Oceanogr.*, *42*(3), 432–442.

Ulshöfer, V. S., G. Uher, and M. O. Andreae (1995), Evidence for a winter sink of atmospheric carbonyl sulfide in the northeast Atlantic Ocean, *Geophys. Res. Lett.*, *22*(19), 2601–2604.

Vallina, S. M., and R. Simó (2007), Strong relationship between DMS and the solar radiation dose over the global surface ocean, *Science*, *315*(5811), 506–508.

Von Hobe, M., A. Kettle, and M. Andreae (1999), Carbonyl sulphide in and over seawater: Summer data from the northeast Atlantic Ocean, *Atmos. Environ.*, *33*(21), 3503–3514.

Von Hobe, M., G. Cutter, A. Kettle, and M. Andreae (2001), Dark production: A significant source of oceanic COS, *J. Geophys. Res.*, *106*(C12), 31,217–31,226.

Weiss, P., J. Johnson, R. Gammon, and T. Bates (1995), Reevaluation of the open ocean source of carbonyl sulfide to the atmosphere, *J. Geophys. Res.*, *100*(D11), 23,083–23,092.

Whelan, M. E., D.-H. Min, and R. C. Rhew (2013), Salt marsh vegetation as a carbonyl sulfide (COS) source to the atmosphere, *Atmos. Environ.*, *73*, 131–137.

Xiao, Z., S. Liang, J. Wang, P. Chen, X. Yin, L. Zhang, and J. Song (2014), Use of general regression neural networks for generating the GLASS leaf area index product from time-series MODIS surface reflectance, *IEEE Trans. Geosci. Remote Sens.*, *52*(1), 209–223.

Xie, H., and R. M. Moore (1999), Carbon disulfide in the North Atlantic and Pacific oceans, *J. Geophys. Res.*, *104*(C3), 5393–5402.

Xu, X., H. G. Bingemer, H.-W. Georgii, U. Schmidt, and U. Bartell (2001), Measurements of carbonyl sulfide (COS) in surface seawater and marine air, and estimates of the air-sea flux from observations during two Atlantic cruises, *J. Geophys. Res.*, *106*(D4), 3491–3502.

Zepp, R., and M. Andreae (1994), Factors affecting the photochemical production of carbonyl sulfide in seawater, *Geophys. Res. Lett.*, *21*(25), 2813–2816.